Available online at www.sciencedirect.com
SCIENCE DIRECT®
Chemical Physics Letters 365 (2002) 69–74
CHEMICAL PHYSICS LETTERS
www.elsevier.com/locate/cplett

Pore structure of raw and purified HiPco single-walled carbon nanotubes

Martin Cinke [1], Jing Li [*,1], Bin Chen [1], Alan Cassell [1], Lance Delzeit, Jie Han [1], M. Meyyappan

NASA Ames Research Center, Center for Nanotechnology, M/S 229-1, Moffett Field, CA 94035, USA

Received 30 July 2002; in final form 4 September 2002

Abstract

Very high purity single-walled carbon nanotubes (SWNTs) were obtained from HiPco SWNT samples containing Fe particles by a two-step purification process. The raw and purified samples were characterized using high resolution transmission electron microscopy (HRTEM), Raman spectroscopy and thermogravimetric analysis (TGA). The purified sample consists of ~0.4% Fe and the process does not seem to introduce any additional defects. The N_2 adsorption isotherm studies at 77 K reveal that the total surface area of the purified sample increases to 1587 m^2/g from 567 m^2/g for the raw material, which is the highest value reported for SWNTs.

1. Introduction

Single-walled carbon nanotubes (SWNTs) have been receiving much attention due to their remarkable mechanical properties and unique electronic properties. Bulk nanotubes have been investigated in high strength composites [1,2], gas storage [1,3–6] and high surface area catalysts [7] and their potential in all these areas appears to be promising. These applications require availability of large quantities of SWNTs at reasonable prices, and large scale production processes are under development across the world. A high pressure CO disproportionation (HiPco) process is one such development [8,9] to meet the increasing demand for SWNTs. This process is based on the decomposition of $Fe(CO)_5$ to form iron clusters for the catalytic production of SWNTs from CO at about 1000 °C. Early production results [8,9] indicated an iron content of up to 30% by weight and this group has also reported a purification protocol [10]. Several other purification procedures [5,11,12] have reported an iron content of 2–6 wt% for purified HiPCo samples. Du et al. [5] used the purification protocol in [10] and reduced the Fe content to 3.5 wt%. The procedure consisted of an acid treatment to remove the metal, filtration, washing with water, and drying in vacuum; this procedure reportedly reduced the percentage of the open pores available in the raw samples, as shown by Ar adsorption isotherms. Yudasaka et al. [11]

* Corresponding author. +1-650-604-4352.
E-mail address: jingli@mail.arc.nasa.gov (J. Li).
[1] Eloret Corporation.

0009-2614/02/$ - see front matter
PII: S0009-2614(02)01420-3

found that high vacuum heat treatment of HiPco tubes for 5 h at 2000 °C reduces Fe content to 2% while the diameter of SWNTs increased substantially. The mechanism for the diameter swelling was not presented. This group also performed [12] a different purification approach for the HiPco material with HCl-washing after air oxidation which provided a purified sample with 6 wt% iron. This sample showed a 65% increase in the total surface area (861 m^2/g) compared to the raw material, as determined by N_2 adsorption isotherms.

In general, the reported surface area for SWNTs in the literature until now is not high. Luo et al. [7] measured a BET (Brunauer–Emmett–Teller) surface area of 180 m^2/g for SWNTs prepared by CO disproportionation followed by HNO_3 treatment and air oxidation. SWNTs from an arc discharge process, after HCl treatment, were shown to have a surface area of 483 m^2/g [6]. Basca et al. [13] obtained 790 m^2/g for a sample that contained single- and double-walled nanotubes. Other studies indicate a BET area of only 15–250 m^2/g, as summarized in [14]. Compared to these, the measurements by Du et al. [5] on the purified HiPco samples exhibit the highest surface area to date at 861 m^2/g. Surprisingly, these values are lower than the surface areas of commercially available activated carbons ($\sim$1000 m^2/g) while theoretical estimates [14] for SWNTs seem to be much higher; for example, Monte Carlo molecular simulations show a BET area as high as 3000 m^2/g for open nanotubes of 3 nm diameter with a 0.4 nm spacing between the walls of two adjacent tubes. This indicates a need for improved methods to purify the as-grown nanotubes and open the ends in order to improve the adsorptive capacity.

In the present work, we use a two-step purification procedure for the HiPco SWNTs that reduces the iron content to <1 wt%. The first step is designed to debundle the nanotube ropes by a dimethylformamide (DMF)/ethylene diamine (EDA) treatment. The second step involves a HCl treatment and wet oxidation to remove metals and amorphous carbon, thus opening the pores. N_2 adsorption studies reveal nearly a factor of 3 increase in the total surface area for the purified material. We have obtained a surface area of 1587 m^2/g which is the highest reported for SWNTs to the best of our knowledge. Large surface areas and pore volumes are advantageous in gas storage applications, catalyst development and waste removal by adsorption. An example of the latter is the processing of CO, NO_x, etc from crew cabins in long duration space flights.

2. Experimental work

Step 1: A solvent mixture of 200 ml DMF (Aldrich, 99.9%) and 100 μl EDA (Aldrich, 99+%) was used to suspend 100 mg raw HiPco SWNTs and this solution was stirred for 18 h followed by a 6.5 h sonication. The solution was then centrifuged and the solvent mixture was decanted. The precipitates were centrifuged and decanted twice with methanol as the washing solvent. The entire procedure was repeated once more. The amine and amide groups in these solvents can interact with the π-electrons on the surface of the carbon nanotubes. Therefore, this procedure helps to loosen the nanotube bundles.

Step 2: Next, the DMF/EDA-treated SWNTs were suspended in 250 ml of 37% HCl (Aldrich) and sonicated for 15 min to get the nanotubes dissolved. The stirred solution was heated to 45 °C for 2 h. The solution was then diluted with double distilled water and cooled to room temperature because the centrifuge tubes cannot tolerate a high concentration of acid. The solution was centrifuged and decanted four times with double distilled water. The SWNTs were dried in air and placed in a quartz boat located at the center of a quartz tube connected to a water bubbler. A stream of wet air was fed into the quartz tube with the tube maintained at 225 °C for 18 h and then the SWNTs were cooled to room temperature. The HCl treatment removes the metals and the wet air oxidation removes the amorphous carbon. This aspect of the purification procedure (i.e., the entire step 2) was repeated three more times, but with the wet air oxidation part modified slightly each time (325 °C for 1.5 h; 425 °C for 1 h; skipping the step, respectively).

High resolution transmission electron microscopy (HRTEM) was used at various stages of the purification process to keep track of the quality of the SWNTs. The samples were also analyzed using

Raman spectroscopy as described in [15]. Thermogravimetric analysis (TGA) (Perkin-Elmer TGA Pyris 1) was performed to determine the impurities, and decomposition temperature and rate. The sample was loaded in a platinum pan for weight loss measurement. The sample was burned with a ramping rate of 25 °C/min in the temperature range 50–1025°C. Ambient air with 20 ml/min was used as carrier gas for characterizing the metal impurities. The nanopore structures were determined by adsorption of N_2 at 77 K using Micromeritics ASAP 2010 surface analyzer. The sample was loaded in a quartz tube evacuated to 10^{-6} Torr and cooled with liquid nitrogen to 77 K. N_2 gas (99.9995%) was incrementally released into the quartz tube for adsorption measurements at different relative vapor pressures. Calculation of surface area, pore size distribution, and pore volumes was done from this characterization as outlined in [16].

3. Results and discussion

Fig. 1 shows HRTEM images and Raman spectroscopy results for raw HiPco material and purified samples after the two-step process. TEM images show particles of Fe or carbon-coated Fe in the raw material while these are not seen in the purified sample. Raman spectra in the high frequency region show tangential mode D band at 1335 cm^{-1} as well as characteristic narrow G band around 1585 cm^{-1}. The D band structure may be due to the amorphous carbon introduced during growth as well as nanotubes with open caps or wall defects. The intensity ratio I_G/I_D increases slightly, after the two-step purification process, due to the removal of amorphous carbon and opening of the gaps. The curve fitting results indicate an increase in the 1547 cm^{-1} component, commonly believed as the contribution from nanotubes of smaller chiral angles [17]. It is possible that some of the SWNTs undergo preferential reconstruction as an annealing process. There is no indication that the purification steps create any new defects.

The diameter distribution estimated from the radical breathing modes (RBM) ranges from 0.93 to 1.35 nm. The peaks corresponding to diameters of 0.94, 1.01, 1.10 and 1.16, 1.22, 1.35 are seen. A change in relative intensity for various peaks in the

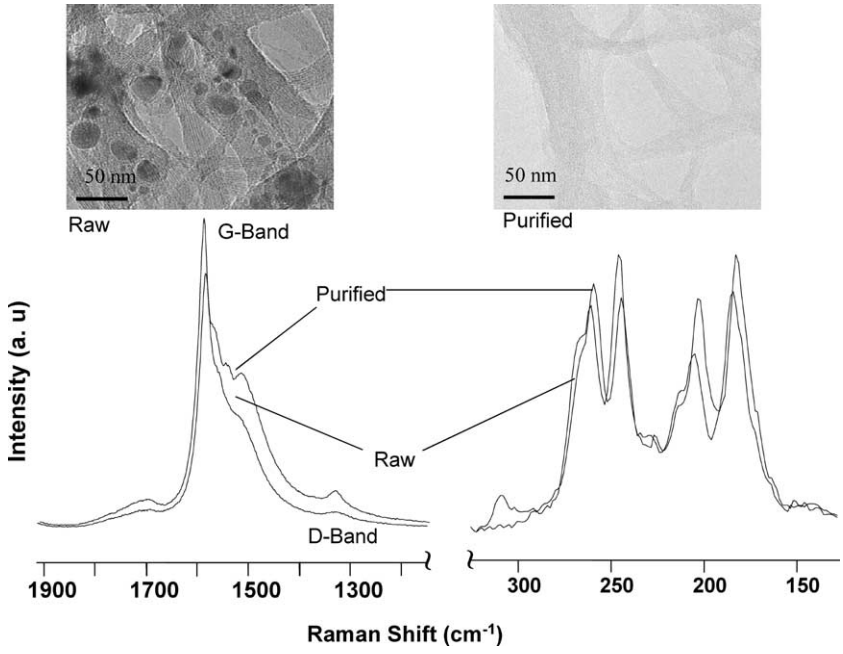

Fig. 1. HRTEM images and Raman spectroscopy results (514 nm excitation) for raw and purified HiPco SWNTs.

RBM region has been observed (both 514 and 782 nm excitation) indicating the ratio of small diameter nanotubes has increased after purification relative to larger diameter tubes. Such a change has been reported previously [10,18]. Another interesting observation is that the spectra, both in tangential and RBM regions, are blue-shifted by about 10 cm^{-1} after the purification. This may be related to a decrease in internanotube interaction after the bundles are dispersed by the DMF/EDA treatment.

The TGA results (Fig. 2) indicate a 22 wt% Fe content in the raw HiPco material which dropped to 0.4% after the two-step purification process. The early weight gain in the raw material is due to conversion to metal oxides. The metal impurities in the raw material lower the decomposition temperature and increase the decomposition rate. The purified material with very little metal is thermally more stable towards oxidative destruction than the raw SWNTs. Experiments also show that longer sonication periods resulted in lowering the decomposition temperature and raising the rate as expected due to the resulting shorter fragments of nanotubes.

Fig. 3 shows N_2 adsorption isotherms for the raw HiPco material and a sample purified using the complete two-step process. For comparison, an isotherm for a sample that was subjected only to Step 2 (HCl treatment and wet oxidation) is also shown; step 2 alone is similar to the procedure in [10]. All isotherms are clearly of Type IV showing a hysterisis loop at high values of P/P_0 [16]. In the intermediate pressures, the uptake of N_2 gradually increases with P/P_0. The adsorptive capacity improves significantly as expected upon purification. At $P/P_0 = 0.2$ for example, the volume adsorbed increases from 161 cm^3/g STP for the raw material to 441 cm^3/g STP for the completely purified sample. The 2.75-fold increase in capacity matches the increase in BET surface area discussed below. It is also evident that a substantial fraction of this improved capacity can be attributed to the debundling effects of the DMF/EDA treatment. The peak capacity at P/P_0 reaches 1000 cm^3/g STP ($= 1250$ mg/g) for the purified sample.

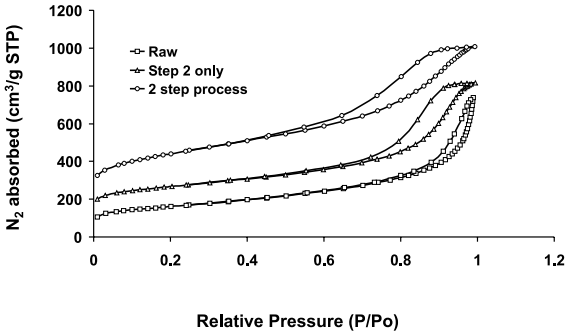

Fig. 3. N_2 adsorption isotherms (77.6 K) for the raw SWNTs and a sample purified using the complete two-step process. Isotherm for a sample which skipped Step 1 (DMF/EDA treatment) and was subjected only to the HCl treatment/wet oxidation (Step 2) is also shown for comparison.

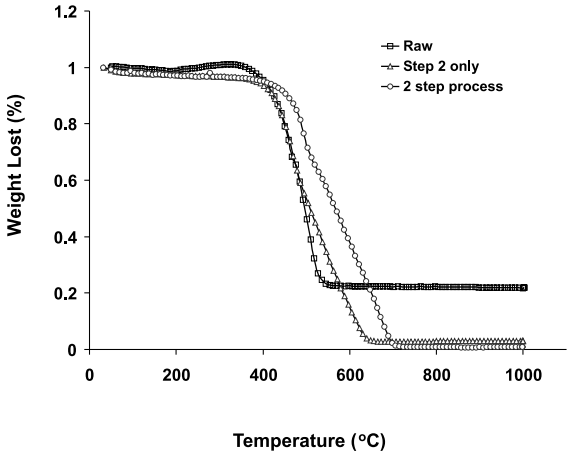

Fig. 2. Thermogravimetric analysis results.

Fig. 4 presents the pore distribution data corresponding to the N_2 adsorption isotherms in

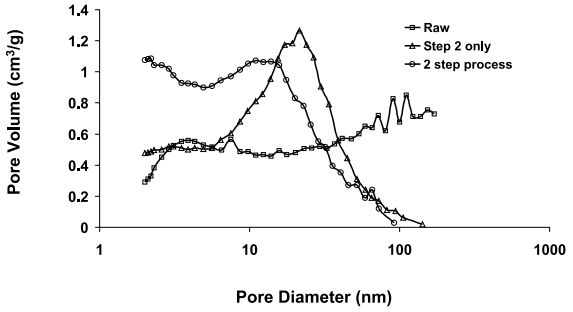

Fig. 4. Pore distribution corresponding to Fig. 3.

Table 1
Nanostructural properties of raw and purified SWNTs

Sample	Total surface area (BET) (m^2/g)	External area (m^2/g)	Internal area (m^2/g)	Total pore volume (ml/g)	Mircopore volume (ml/g)	Average pore size (nm)
Raw SWNTs	577	382	194	1.06	0.08	7.4
Step-2 only	968	506	461	1.26	0.19	5.2
Complete two-step process	1587	909	678	1.55	0.28	3.9

Fig. 3. The computed pore structure properties are listed in Table 1. The total BET surface area of raw HiPco is 577 m^2/g which compares with a value of 524 m^2/g for HiPco material previously reported by Yang et al. [12]. Any minor differences in the raw material properties between our data and those of [5] and [12] may be attributed to batch-to-batch variations of a process that is constantly undergoing improvements. Remarkably the total surface area of our completely purified sample is 1587 m^2/g which is nearly twice that of the previous best values for HiPco or other SWNTs (861 m^2/g in [12]). If the DMF/EDA treatment is skipped and only the acid treatment/wet oxidation is performed, we only see a total area of 968 m^2/g. It is clear that the debundling process by the DMF/EDA treatment is effective in increasing the external area as well as the efficiency of the metal and amorphous carbon removal process of the loosened bundles. The total pore volume also increases upon purification. Both Fig. 3 and Table 1 reveal the presence of micropores. The mesopores, obtained by subtracting the micropore volume from the total, constitute the major fraction of the pores. There is a significant number of pores of diameter >30 nm in the raw sample, yielding an average pore size 7.4 nm. The purification process results in pores of much smaller size (see Fig. 4) pushing the average pore size down to 3.9 nm.

Yin et al. [14] presented Monte Carlo molecular simulations of N_2 adsorption at 77 K for nanotubes of 0.6–3 nm diameter and internanotube separation of 0.4–3 nm. Although they considered a square array, which is a highly contrived scenerio, their results reveal interesting insight into adsorption mechanisms. For a given SWNT diameter, the adsorptive capacity increases with nanotube separation according to their simulations. Yin et al. [14] parametrized their simulation results for adsorptive capacity at $P/P_0 = 1$ as:

$$w\ (\mathrm{mmol/g}) = 9.146 f \left[\frac{D}{\pi} \left(1 + \frac{G}{\mathrm{D}} \right)^2 - \sigma_{\mathrm{cc}} \right],$$

where f is a packing parameter (taken as 0.415 from Fig. 12 in [14]), D and G are nanotube diameter and separation in Angstroms, and σ_{cc} is the Lennard-Jones length parameter for carbon–carbon interaction (3.769 Å). If we take an average diameter of 1.1 nm and a conservative G/D of 1.0 to represent our results, then we get an adsorption capacity of 38.9 mmol/g (871 cm^3/g STP). The experimental results from Fig. 3 is about 1000 cm^3/g STP.

4. Concluding remarks

Applications such as gas adsorption, catalysis, storage of H_2, Li and other metals have been speculated since the discovery of SWNTs. All these applications require high specific areas and pore volumes. The BET surface area of SWNTs reported in the literature have been small. Recent availability of HiPco SWNTs promises to provide bulk quantities of large surface area material. We have presented a two-step purification, first to debundle the nanotubes with a DMF/EDF treatment and a second step of acid treatment followed by wet oxidation. This procedure has yielded SWNTs with a BET area of 1587 m^2/g which is the highest value reported for nanotubes.

Acknowledgements

Work by ELORET authors is supported by a NASA contract to ELORET. The authors

acknowledge Christina Binder for her TGA work. Professor R.E. Smalley is gratefully acknowledged for providing HiPco samples.

References

[1] P.M. Ajayan, O. Zhou, in: M. Dresselhaus, G. Dresselhaus, P. Avouris (Eds.), Carbon Nanotubes, Springer, Berlin, 2001, p. 391, see references therein.
[2] P.A.O.' Rourke Meisner, L. Clayton, J.D' Angelo, J.P. Harmon, A.K. Sikdar, A. Kumar, A.M. Cassell, M. Meyyappan, J. Mater. Res., (2002).
[3] Y. Ye, C.C. Ahn, C. Witham, B. Fultz, J. Liu, A.G. Rinzler, D. Colbert, K.A. Smith, R.E. Smalley, Appl. Phys. Lett. 74 (1999) 2307.
[4] Y. Ma, Y. Xia, M. Zhao, R. Wang, L. Mei, Phys. Rev. B 63 (2001) 115422.
[5] W. Du, L. Wilson, J. Ripmeester, R. Dutrisac, B. Simard, S. Denommee, NanoLetters 2 (2002) 343.
[6] M. Eswaramoorthy, R. Sen, C.N.R. Rao, Chem. Phys. Lett. 304 (1999) 207.
[7] J.Z. Luo, L.Z. Gao, Y.L. Leung, C.T. Au, Catal. Lett. 66 (2000) 91.
[8] P. Nikolaev, M.J. Bronikowski, R.K. Bradley, F. Rohmund, D.T. Colbert, K.A. Smith, R.E. Smalley, Chem. Phys. Lett. 313 (1999) 91.
[9] M.J. Bronikowski, P.A. Willis, D.T. Colbert, K.A. Smith, R.E. Smalley, J. Vac. Sci. Technol. A 19 (2001) 1800.
[10] L.W. Chiang, B.E. Brinson, A.Y. Huang, P.A. Willis, M.J. Bronikowski, J.L. Margrave, R.E. Smalley, R.H. Hauge, J. Phys. Chem. B 105 (2001) 8297.
[11] M. Yudasaka, H. Kataura, T. Ichihashi, L.C. Qin, S. Kar, S. Iijima, NanoLetters 1 (2001) 487.
[12] C.M. Yang, K. Kaneko, M. Yudasaka, S. Iijima, NanoLetters 2 (2002) 385.
[13] R.R. Basca, Ch. Laurent, A. Peigny, W.S. Basca, Th. Vaugien, A. Roussett, Chem. Phys. Lett. 323 (2000) 566.
[14] Y.F. Yin, T. Mays, B. McEnaney, Langmuir 15 (1999) 8714.
[15] L. Delzeit, B. Chen, A. Cassell, R. Stevens, C. Nguyen, M. Meyyappan, Chem. Phys. Lett. 348 (2001) 368.
[16] P.A. Webb, C. Orr, Analytical Methods in Fine Particle Technology, Micromeritics, 1997.
[17] A. Jorio, M.S. Dresselhaus, M. Souza, M.S.S. Dantas, M.A. Pimenta, A.M. Rao, R. Saito, C. Liu, Phys. Rev. Lett. 85 (2000) 2617.
[18] J.L. Bahr, J. Yang, J.V. Kosynkin, M.J. Bronikowski, R.E. Smalley, J.M. Tour, J. Am. Chem. Soc. 123 (2001) 6536.